Book Section:
Jaksic, V., Kennedy, C.R., Grogan, D.M. et al. (2018) Influence of composite fatigue properties on marine tidal turbine blade design. In: Davies, P. and Rajapakse, Y.D.S., (eds.) Durability of Composites in a Marine Environment 2. Solid Mechanics and its Applications, 245. Springer International Publishing, pp. 195-223. ISBN: 9783319651446. ISSN: 0925-0042. EISSN: 2214-7764.

https://doi.org/10.1007/978-3-319-65145-3_11

Influence of Composite Fatigue Properties on Marine Tidal Turbine Blade Design

Vesna Jaksic[1], Ciaran R. Kennedy[2], David M. Grogan[2], Sean B. Leen[2], Conchúr M. Ó Brádaigh[3]

[1] Sustainable Infrastructure Research & Innovation Group (SIRIG), Civil, Structural and Environmental Department, Cork Institute of Technology, Ireland
[2] Department of Mechanical Engineering, National University of Ireland, Galway, Ireland
[3] Institute for Materials and Processes, University of Edinburgh, Scotland, UK

Contact e-mail address:
vesna.jaksic@cit.ie
ciaran.kennedy@nuigalway.ie
sean.leen@nuigalway.ie
c.obradaigh@ed.ac.uk

Contact telephone number: +353 21-4335950

Summary. *The structural design of marine tidal turbine blades is governed by the hydrodynamic shape of the aerofoil, extreme loadings and composite material mechanical properties. The design of the aerofoil, chord and twist distribution along the blade is generated to optimise turbine performance over its life time. Structural design gives the optimal layout of composite laminae such that ultimate strength and buckling resistance requirements are satisfied. Most structural design approaches consider only extreme static loads, with a lack of dynamic loads-based fatigue design for tidal blades. Approaches for tidal turbine blade design based on dry and immersed composite material fatigue life are studied.*

Keywords. Composites, marine environment, fatigue properties, tidal turbine blades, design.

1 Introduction

In order to fully utilise the tidal blade structural material fatigue life it is necessary to have information on its performance in marine environment for the full design life of marine renewable energy devices (10-20 years). To date, however, there are no reports available of experience with heavily loaded GFRP structures operating in this environment. In addition, the literature on fatigue test programs for the composite materials that will be used in marine renewable energy devices is limited. Consequently, designers of these devices are forced to be quite conservative in their structural design, leading to increased cost. A comprehensive fatigue life model for composite blades, incorporating realistic hydrodynamic loadings, cyclically-varying blade stresses and wet composite material fatigue properties, will therefore be very valuable for tidal turbine designers. In this regard, the aim of the study is to quantify the degradation in fatigue strength of composite materials due to water uptake and to predict the degradation in tidal turbine blade life due to water saturation.

1.1 Tidal energy

Tidal energy is gaining increased attention due to its predictable nature as renewable

energy source. The efficiency of tidal power is around 80%, much greater than coal, solar or wind. The geographic distribution of tidal energy resources around the world is presented in Fig. 1 [1].

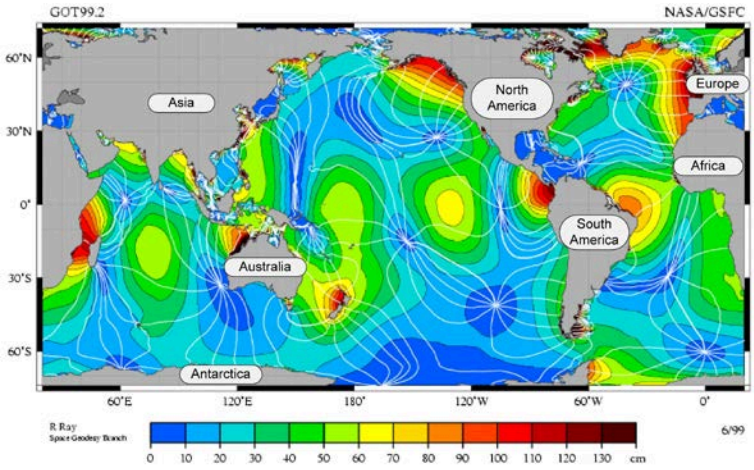

Fig. 1 World tidal energy patterns [1].

The map shows that there is considerable tidal energy-harnessing potential around the coastlines of the UK, Ireland and France, among others. The total theoretical tidal energy resources available in broad geographic areas around the UK (Fig. 2) are estimated to be 216 TWh/year [2] while estimated Irish resources are 230 TWh/year [3]. However, technological limitations, physical, environmental, and commercial constraints will make extraction of all this available energy impossible. However, taking into account the ocean energy projects which have been awarded funds, Europe could see up to about 57 MW of tidal energy capacity installed operational by 2020 [4].

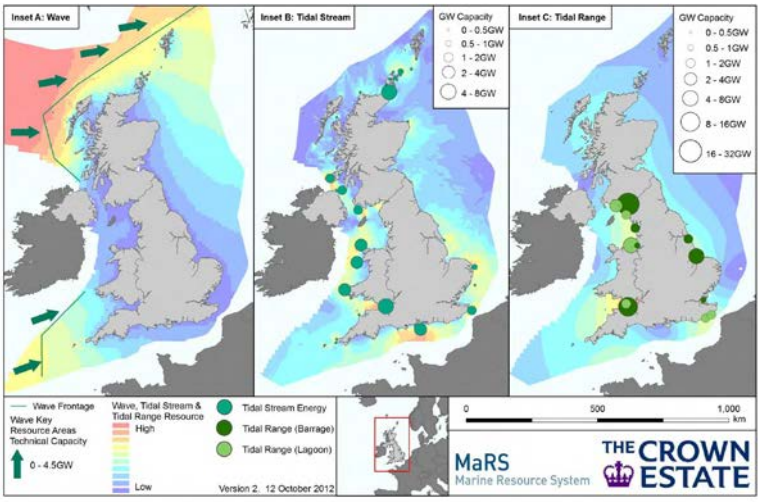

Fig. 2 Wave and tidal power distribution and energy map – UK [2].

1.2 Composite Tidal Turbine Blades

Despite the predictable nature of tides, tidal current intensity and variability over small geographical areas cannot be foreseen [5]. Turbine rotors are the part of tidal device structures that are most sensitive to harsh marine environment, extreme weather and turbulence flows [6; 7], as well as having to withstand erosion due to ice, sand and floating trees. Tidal turbine blades are subject to water ingress and saturation during the device employment period [8]. The blade failures on a number of prototypes highlight the need for

design that will withstand the expected hydrodynamic loads [9; 10]. Experience shows that blade failure due to environmental loading often happens in short periods. Structural health monitoring of tidal blades on seabed-mounted devices in particular, is difficult and expensive and in the case of damage, costly lifting vessels need to be employed.

Hence, tidal blades require high static and fatigue strength. This implies the necessity to use thick composite sections or higher strength reinforcing fibres (carbon). Glass fibre reinforced polymers (GFRP) such as epoxy or vinylester are commonly used for tidal blades due to their good properties, e.g. high strength, corrosion resistance and low cost. However, the research on the potential of using carbon fibre reinforced polymers (CFRP) in tidal blade design [9; 10] is ongoing [11]. The polymers normally used in GFRP can absorb up to 5% water by weight when immersed for long periods and this can reduce the tensile strength of the material more than 25% [12]. Material properties and design impact the life expectancy, and hence energy production from tidal turbines [13]. Furthermore blade development affects the load and cost of other components.

1.3 Modelling of GFRP fatigue life

Composites are a natural choice for turbine blades but there is little test data available on material behaviour under coupled environmental and cyclic loading. An extensive review of modelling of fatigue in GFRP has divided the work into three broad approaches [14]. First is a testing approach where life predictions are based on test data of the exact or similar material, second is the phenomenological approach where predictions are based on the stiffness and residual strength behaviour, and thirdly a progressive damage approach where damage in the unidirectional (UD) lamina is predicted and incremented until a final failure state is reached, thereby predicting fatigue life. The testing approach to fatigue life estimation is by far the most widely used [15; 16]. The technique is constantly being refined to include effects like spectrum loading and complex constant life diagram (CLD) results [17]. Stiffness of GFRP laminates degrades by between 10 and 20% during fatigue cycling. The main drawback of the models discussed up to this point is their lack of flexibility in dealing with different laminate layups and/or loading patterns. Micromechanical approaches that predict the response of the laminate based on damage mechanisms in the individual UD plies offer a potential solution. The simplest approach is to degrade the matrix properties based on observed levels of cracking [18] and use classical laminate theory (CLT) to integrate the results. Others have considered two damage mechanisms, namely matrix cracking and interlaminar delamination [19].

2 Blade Hydrodynamic and Fatigue Model

2.1 Tidal Turbine Blade Design Assumptions

The preliminary design of the tidal blade assumes that device operates in a steady flow. The device configuration considered for the modelling and benchmarking is based on a wind turbine, i.e. a machine which has a horizontal axis oriented up-tide and has three pitch-regulated (PR) blades [20]. Hydrodynamic design of tidal turbine blades can be expected to follow a similar pattern to that of wind turbine blades [9; 21]. Hence, the Blade Element Momentum (BEM) theory is employed for a blade hydrodynamic modelling [22; 23]. In this regard, a preliminary design methodology is presented, based on a minimum number of input parameters, in order to predict the fatigue life of the blades [24; 25].

2.2 Turbine Blade Fatigue Design Methodology

The preliminary fatigue design methodology for GFRP tidal turbine blades consists of a number of separate models, combined to facilitate the hydrodynamic and structural calculations required (Fig. 3).

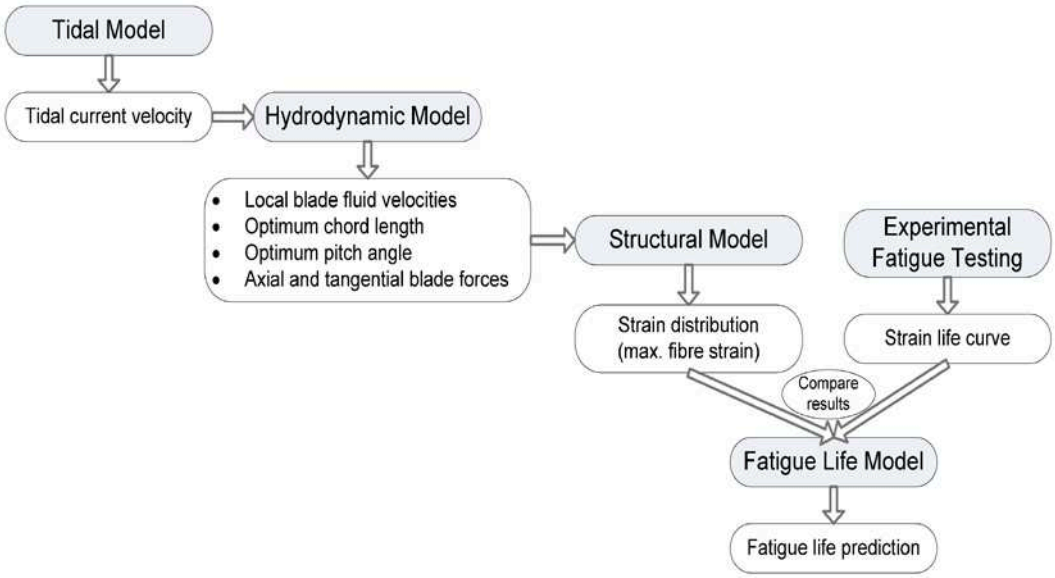

Fig. 3 Algorithm of tidal turbine blade design methodology.

The first module in the design process algorithm is a tidal model which predicts the tidal current speed at any time for specified local tidal velocities [9; 24]. The output from this tidal model forms a key input to a hydrodynamic model, which in turn computes the radial distributions of: local relative blade-fluid velocities, axial and tangential blade forces, optimum chord length, and pitch angle. The subsequent structural module, based on development of a finite element model of the blade, and driven by the output from the hydrodynamic model, is then employed to characterise the strain distribution in the turbine blade. The fatigue model accounts for each rotation of the blade explicitly and determines the maximum strain in the blade for each cycle. It then takes that maximum strain, compares them to experimentally determined strain-life curves for immersed and dry materials and obtains a damage fraction for that cycle [13].

The method can be applied to the preliminary investigation of a number of design aspects for tidal turbines. All of the models used in the methodology are relatively simple and can be quickly processed. This allows adjustment of the key parameters in order to study the effect of changes on the device design and performance. The model takes into the account the experimental results of fatigue testing on GFRP laminates, manufactured using materials and processes which are the current state of the art used in marine renewable energy devices.

2.3 Tidal Model

The tides are the result of interaction of the gravity of the sun, earth and moon. The fall and rise of tides creates kinetic energy. The first module in the design process is a tidal model, which predicts the tidal current speed at any time for specified measured local tidal velocities (Fig. 4). The water speed depends on the local topography, but if the spring (highest tides) and neap (lowest tides) maximum velocities are measured, the full cycle can be approximated by a combination of a semi-diurnal sinusoid and a fortnightly sinusoidal function [26; 27]. The output from the tidal model forms a key input to a hydrodynamic

model.

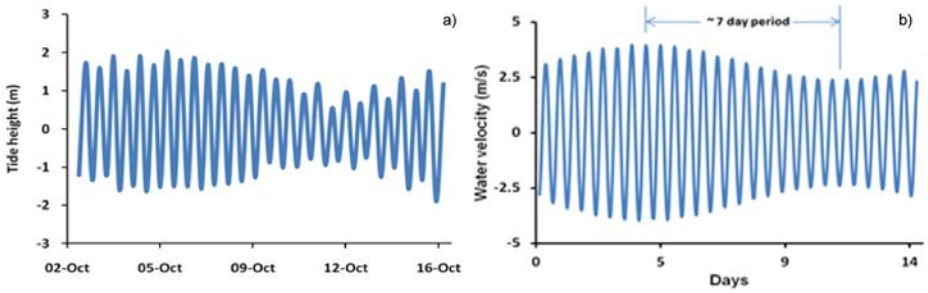

Fig. 4 a) Typical tide height pattern around Ireland [28] and b) Sinusoidal model output for water velocity.

2.4 Hydrodynamic model

The hydrodynamic model (HDM) generates an optimised blade shape for any size turbine when given water velocity (generated by tidal model) and number of blades. It also calculates the forces that are exerted on a the single blade by the water flow. The HDM is based on a streamtube or blade element momentum approach [29; 30] (Fig. 5). Hence, for each streamtube (radial distribution of the blade), local relative blade-fluid velocities, axial and tangential blade forces, optimum chord length, and pitch angle can be calculated. Furthermore, the model predicts the maximum power output, torque and bending moment at the blade root at the chosen water velocity.

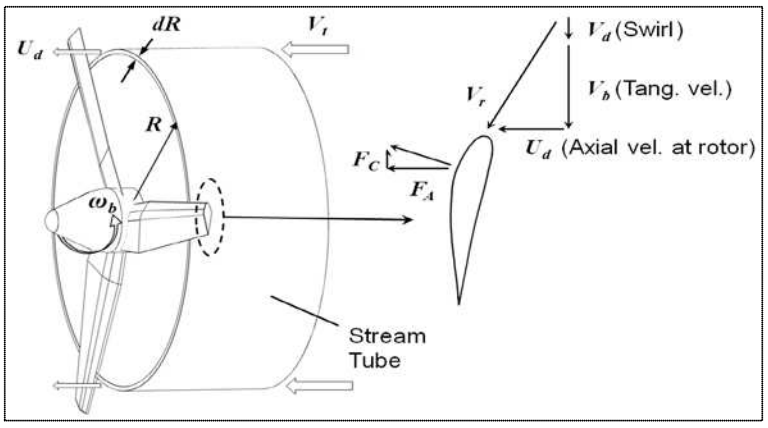

Fig. 5 Schematic of hydrodynamic model concept showing one of the *n* concentrically-stacked stream tube annuli and the associated fluid flows [24].

The lift and drag forces can be estimated to a first order approximation using a stream tube momentum model. The model (Fig. 5), assumes a series of isolated concentric tubes within which momentum loss is in balance with the forces acting on the blade. The fluid forces on the blades (for steady state operation), inside any stream tube, must equal the momentum lost from that stream tube.

The lift force (L), perpendicular and drag force (D), parallel to the fluid velocity, generated by a stream tube on the blade section inside it [24], can be calculated:

$$L = \frac{1}{2} C_L V_r^2 \rho S \Delta R \quad (1)$$

$$D = \frac{1}{2} C_D V_r^2 \rho S \Delta R \quad (2)$$

where C_L and C_D are the coefficients of lift and drag for the aerofoil selected [31], V_r is apparent or relative velocity seen by the blade (Fig. 5), ρ is the density of the fluid, S is the chord length of the blade at the stream tube radius and ΔR is the radial thickness of the stream tube. The axial (thrust) force, F_A and the tangential (torque) force, F_C acting on the blade by observed stream tube can be obtained:

$$F_A = L\cos\theta + D\sin\theta \quad (3)$$

$$F_C = L\sin\theta + D\cos\theta \quad (4)$$

where θ is the angle between the relative velocity and the plane of the rotor.

The input data for the HDM are: water velocity, density, viscosity and initial velocity at the exit, number of blades, outer and inner diameter of the stream tube, RPM, C_L, and lift to drag ratio. Fig. 6 shows an example of the radial distributions of F_A and F_C versus radius as predicted by the hydrodynamic model. Control systems have a significant effect on the forces and moments in a tidal turbine blade, by regulating the power absorbed by the turbine during high water velocity operation.

Fig. 6 Radial distributions of axial (F_A) and tangential (F_C) forces from hydrodynamic model at 2.6m/s water velocity.

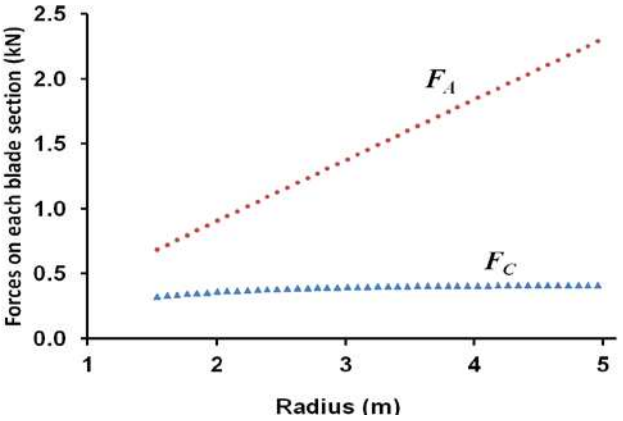

2.5 Finite Element Analysis Model (Static)

A finite element model (FEM) in conjunction with a fatigue life model (FLM) is used to characterise the strain distribution (i.e. maximum strain) in the turbine blade and estimate blade fatigue life. The example of the FEM modelling of tidal blade is given in Fig. 7.

Fig. 7 Finite element model of a tidal blade (top) and flapwise deflection of the blade due to a tidal stream velocity.

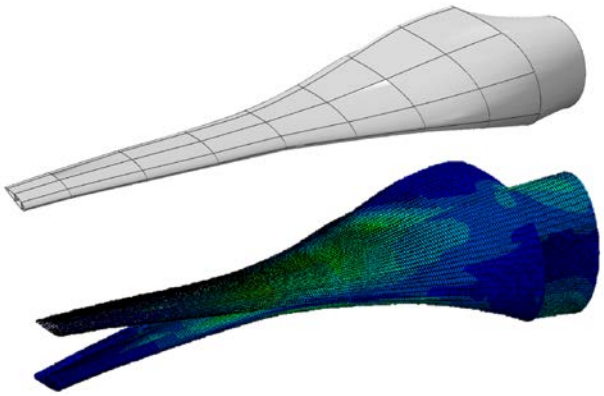

The maximum strains at each blade section are calculated [9] using the stiffnesses predicted from the software code PreComp [32] and the bending moment distributions

predicted by the hydrodynamic model. The flapwise strains in the spar caps are significantly larger than the edgewise strains due to the large thrust forces on the blade. This static design approach can be used to compare the efficiency of using carbon fibre reinforced polymers (CFRP) with the baseline GFRP. An example of predicted flapwise strain distribution along a 12m length blade, for extreme and normal load cases, shows greater strain for the GFRP than for the CFRP sparcaps (Fig. 8). The research shows that even when using thicker laminates (over 100mm), the calculated strains are of the same magnitude as the failure strains of the material. Hence, the risk of failure over the lifetime of the turbine is significant [9]. The use of CFRP increases the static margin of safety in the blade, when compared to GFRP. This becomes important since high tidal velocities (up to 4m/s) could occur and the effect of seawater degradation of the fibre matrix interface is likely to reduce the stiffness of the GFRP over the lifespan of such a device [8; 33]. Hence, the stiffness of the blade can be improved and the mass reduced by introducing a CFRP sparcap, for instance.

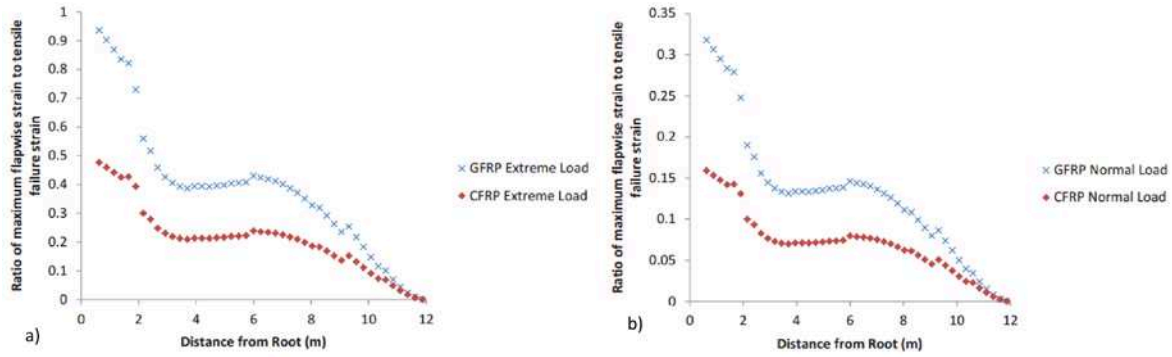

Fig. 8. Maximum flapwise strain in the blade's spar caps, using GFRP and CFRP, calculated using PreComp [34] for tidal stream velocities of (a) 4.1m/s and (b) 2.4m/s [9].

2.6 Fatigue Loading of Blades

The fatigue model focuses on the highest tensile strain in the blade, which is predominantly attributed to the flapwise bending-induced strain. Each cycle of the tide (2 per day) causes a slow increase and then a decrease in the maximum strain on the blade. The blade experiences a cyclic load for each revolution of the machine, caused by the blocking ('shadow') effect of the support tower (Fig. 9).

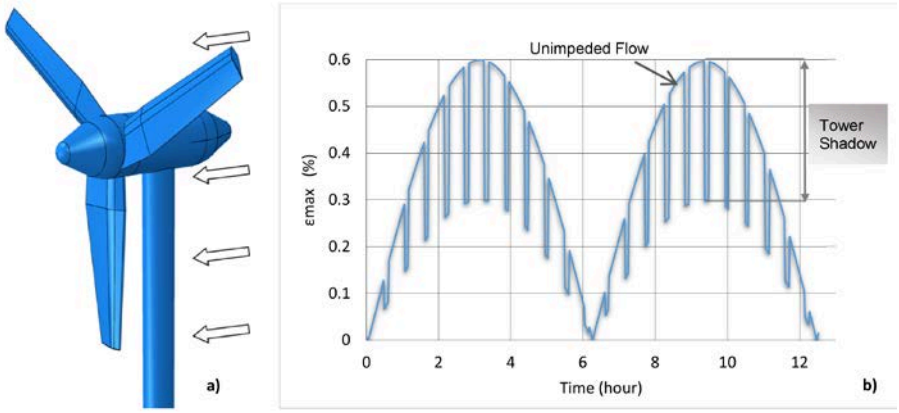

Fig. 9 a) Tower shadow on downstream 3 bladed tidal turbine and b) Schematic of tower shadow effect (50%) on maximum strain in the turbine blade.

Experiments with scaled models of tidal turbines in a wave tank have found flapwise bending moment amplitudes of 50% [35]. This corresponds to a fatigue loading R-ratio ($\varepsilon_{Min}/\varepsilon_{Max}$) of 0.5 [24].

2.7 Blade Fatigue Model

The major strains in the blade are directly proportional to the flapwise bending moment, considering the material in the turbine blade to be essentially linearly elastic. Therefore, the maximum strain at any time j is:

$$\varepsilon_{max,j} = \varepsilon_{max,sp}\left(\frac{M_f(v_j)}{M_{ref}}\right)^2 \quad (5)$$

where $M_f(v_j)$ represents the functional dependence of bending moment on tidal current velocity, M_{ref} the reference bending moment and ε_{ref} the maximum strain in the blade when the reference moment is applied corresponding to a specific reference velocity V_{ref}. The fatigue model has two components caused by two types of load (strain cycles). The first sums the damage due to the strain cycles caused by the low-frequency semi-diurnal tidal cycle, which implicitly includes the lower frequency 14-day tidal cycle effect, while the second is caused by the higher frequency cycles, due to the tower shadow effect.

3 Finite Element Analysis (Damage Model)

In the FE model of the blade, for a particular integration point, the damage fractions are summed to find the 7-day damage and hence the turbine life, using a Miner's rule approach [36]:

$$D_{7-day} = \sum_{k,tide}^{N_7-day}\frac{1}{N_{f,k}} + \sum_{j,rev}^{N_7-day}\frac{1}{N_{f,j}} \quad (6)$$

where N_k is the number of tidal movements during the 7-day period, N_j the number of turbine revolutions during the 7-day period, $N_{f,k}$ and $N_{f,j}$ the numbers of cycles to failure for a given combination of mean and alternating strain during each tide and revolution, respectively, k is the increment of tidal cycles, and j the increment of revolutions of the turbine. Hence, the blade life in years can be obtained:

$$Blade\ life_{years} = \frac{7.38}{365.25 D_{7-day}} \quad (7)$$

where 7.38 is the exact length of the 7-day period used (1/4 of a synodic month) and 365.25 the length of a year in days.

4 Manufacturing and Testing

The structural properties of GFRP materials depend on orientation of the fibres, polymer type and fibre/polymer volume fraction. One of the main advantages of fibre reinforced materials is the ability to align the strong, stiff fibres with the main loads and thereby use the material to its maximum advantage. There are situations, however, particularly in relation to emerging technologies e.g. marine renewable energy, where the loads are not very well understood and are complex and multi-directional in nature, for which quasi-isotropic (QI) laminates can be used.

The multidirectional nature of laminates complicates the fatigue damage mechanisms. Matrix cracking parallel to the fibres or inter fibre failure (IFF) is first seen in the most off-axis plies under tensile loading. Ultimate IFF cracking takes place in the first 25% of fatigue life and the significant drop in stiffness is complete with only a minor reduction in stiffness after this point. However, fatigue strength reductions do not follow the changes in static strength since the damage mechanisms are different in fatigue [37].

4.1 Coupon Manufacture

The Vacuum Assisted Resin Transfer Moulding (VARTM) process was used to lay up 800mm squares of $[(45°/135°/90°/0°)_2]_s$ laminates infused with epoxy or vinyl-ester resin using (Fig. 10a).

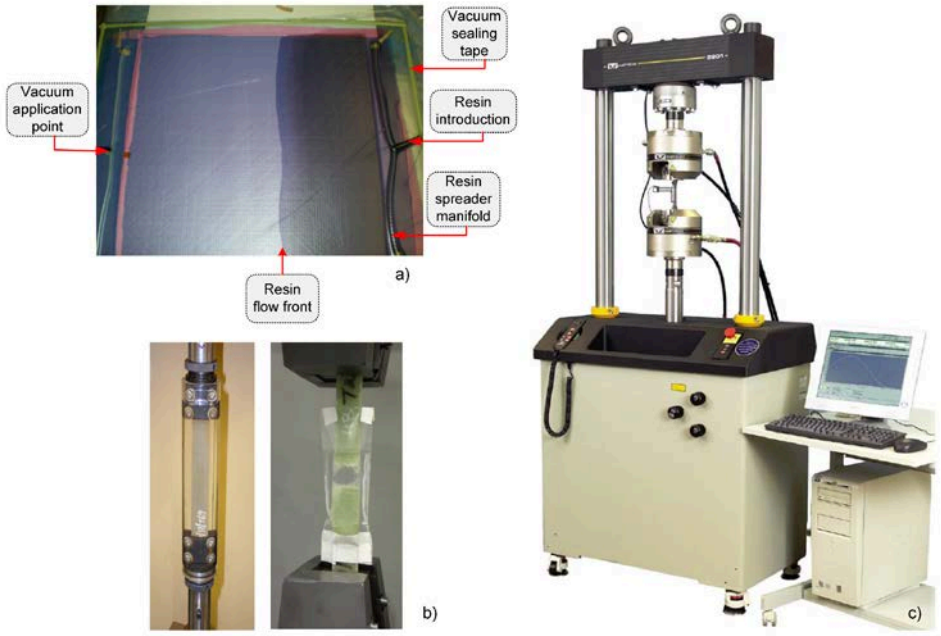

Fig. 10 Coupon manufacturing and testing. a) Vacuum assisted resin transfer moulding process; b) Saturated specimens immersed in tap water (using acrylic tube with O-ring seal and polythene pouch with waterproof tape) during testing; and c) Instron 8801 fatigue test machine.

The E-glass fabric used (Ahlstrom #42007, Ahlstrom Corporation, Helsinki, Finland) is a biaxial non-crimp form with 2 plies (each 300g/m^2) stitched together at 90°, while the 45°/135° plies were obtained by cutting an 800 mm square at a 45° angle biaxial fabric used for the 0°/90° plies. Eight layers of the fabric were stacked on the mould to create the 16 ply laminate. Resin feed tubes, vacuum tubes and spreader manifolds were placed on top of the stack of fabrics and a layer of breather fabric laid over the top of the entire surface to provide a path for the resin to spread across the laminate. A vacuum bag was laid over and sealed around the edges of the mould with a synthetic rubber sealant tape and the resin feed and vacuum tubing were brought out through the seal. The vinyl-ester resin, Scott Bader VE676-03 (Scott Bader Company Ltd., Wellingborough, UK), was mixed with 2% Accelerator G, then 2% Trignox 239 catalyst (Akzo Nobel N.V., Amsterdam, The Netherlands) was added and mixed thoroughly. The resulting mixture was allowed to stand for 5 minutes to de-gas before introduction into the fabric stack. It took approximately 25 minutes, at 18°C room temperature, to infuse into the 0.8 m × 0.8 m × 3.75 mm laminate. The process was repeated to manufacture the epoxy/E-glass laminates (the hand lamination

formula of Ampreg 22 with slow hardener - Gurit Holding AG, Wattwil, Switzerland). Since this resin is more viscous than is optimum for resin infusion, the viscosity was lowered by increasing the temperature to 27°C and it took an hour to infuse into the laminate.

The vacuum continued to be applied for a number of hours after infusion, until the resin had set and after a room temperature cure for 48 hours, the laminates were oven cured at 80°C for approximately 4 hours. Fibre volume fractions of 50% were achieved at an average thickness of 3.75 mm. The laminates were cut into 25×250 mm coupons (Fig. 10b) using a water cooled, diamond-tipped, rotary saw under controlled feed rate.

4.2 Fatigue testing

An Instron 8001 test machine with 8800 controller was used for fatigue testing (Fig.10b&c), applying a sinusoidal force-time history in tension-tension mode (R=0.1), at frequencies of between 3 and 6 Hz. All static tests and a small number of fatigue tests were carried out on an Instron 8500 test machine with an 8800 controller. The gripping pressure on both machines was adjusted to 50 MPa and 100 MPa for fatigue and static tests, respectively. The fatigue test frequency was decreased to maintain a constant rate of strain application as the strain level increases ensuring that the coupon does not overheat. A fan was also used to cool the coupon during testing. A radiation thermometer measured less than 10°C temperature rise in surface temperature during the highest stress cycling test. The temperature in the test room with the 8001 machine was maintained at 21°C and with the 8500 machine varied between 15° and 19°C. Five coupons were tested at each of four separate stress levels (Fig. 10c). Approximately twenty coupons of each material were tested over a range of maximum stress levels that caused the coupons to fail between 100 and 10 million cycles. The number of cycles to failure and the maximum fatigue strain applied to each coupon was recorded, producing a strain-life (ε-N) curve. A power law relationship between maximum initial strain ($\varepsilon_{max,i}$) and fatigue life is

$$\varepsilon_{max,i} = AN_f^{-B} \tag{8}$$

where N_f is the number of cycles to failure, and A and B are constants for power law fit to fatigue data.

Vinyl ester/E-glass has a number of advantages over the epoxy/E-glass material used, e.g. lower cost and increased resistance to water penetration. However, the epoxy resin shows superior fatigue performance over the vinyl ester resin. The strain–life fatigue test results for the epoxy/E-glass and vinyl ester/E-glass materials along with the corresponding power law curve fits, equation (8), are presented in Fig. 11. During the testing, epoxy proved to be more tolerant to the cracks and minor delaminations (appear at the edges of the coupon during testing). Furthermore, applying experimental fatigue data for both of the materials in the fatigue model and integrating with respect to time history of tidal velocity, it is predicted that the maximum strain in a vinyl ester blade must be 29% less than in an epoxy blade, to achieve the same fatigue life.

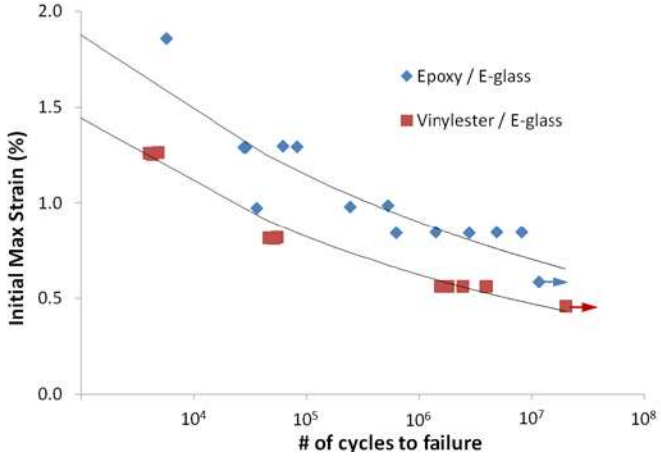

Fig. 11 Test results for Quasi-Isotropic (QI) laminates (R = 0.1).

5 Effects of Water Saturation

GFRP tends to absorb a small amount of water, typically less than 5% [12]. The water diffuses into the polymer matrix, changing its mechanical properties. The water fills any small voids and tends to dilute any unreacted constituents of the polymer, while the resulting osmotic pressure can cause damage to the laminate, i.e. stress corrosion cracking (SCC) of the fibres may occur.

The materials and processes have been chosen to create state of the art GFRP laminates in order to perform accelerated ageing on these laminates at a low temperature, and testing in order to reliably mimic the water saturation level found in an operating tidal turbine blade as described in Section 4.1.

5.1 Accelerated Ageing Procedure

Accelerated ageing was used to simulate the effect of approximately 20 years in cold seawater by immersing the QI specimens, with either epoxy or vinyl-ester matrix reinforced with E-glass or E-CR glass (Table 1), in warm (30 to 40°C) water for up to 2.5 years [13]. Movement of moisture by diffusion into the polymer resin and damage processes within the composite were accelerated by increasing the temperature of the material.

Figure 12 shows a plot of the acceleration factors for epoxy with the diffusion constant that result from combinations of operating (reference) temperatures and accelerated ageing temperatures [38]. 12°C has been chosen as the design operating temperature for a tidal turbine operating off the coast of Ireland. The graph shows that the 20°C and 30°C ageing temperatures will cause diffusion-controlled processes in epoxy/E-glass composites to proceed approximately 3 and 10 times faster, respectively, than at the 12°C operating environment. The water temperature for vinyl-ester ageing was increased to 40°C, which results in an acceleration factor of 10 [13; 38]. Hence, immersing vinyl-ester glass composite in a water bath at 40°C for one year will cause damage equivalent to 10 years in 12°C seawater.

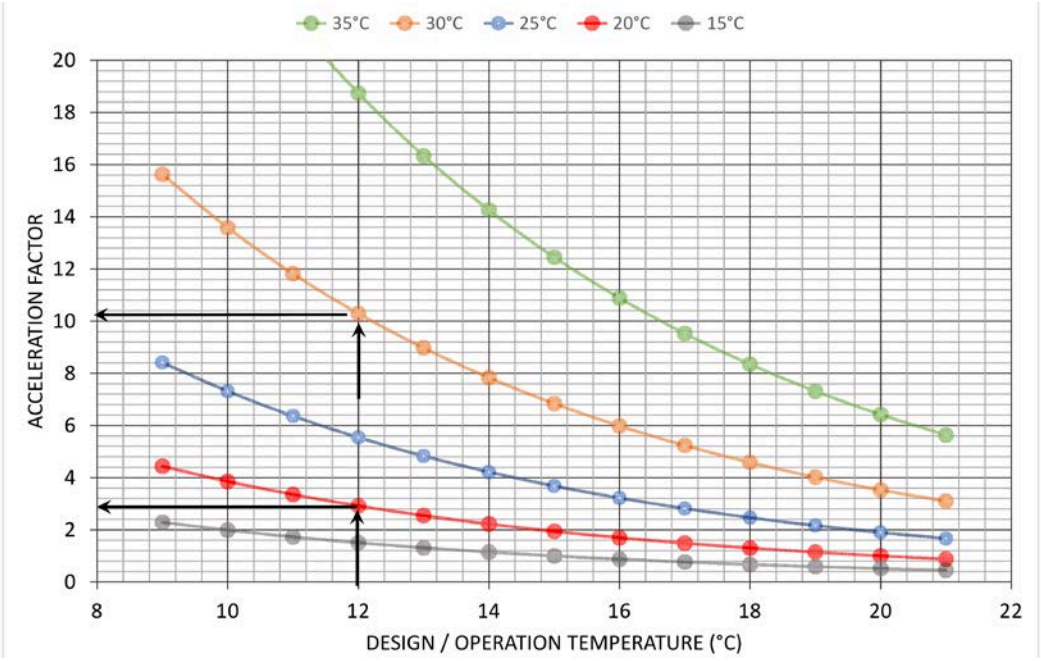

Fig. 12 Predicted acceleration factor for epoxy/E-glass composite due to ageing water temperature.

Table 1. The list of the materials tested and ageing procedures used.

Material	V_f	Thickness	Immersion ageing	Stress Aged
Vinyl ester/E-glass	50% ±2%	3.75 mm	40°C / 30 mths	21 mths
Vinyl ester/E-CR glass	60% ±2%	4.22 mm	40°C / 20 mths	
Epoxy/E-glass	50% ±2%	3.75 mm	30°C / 29 mths	

Two tap water baths with heater-stirrers (heated water is distributed throughout the entire tank) were used during the specimen age-immersion proces. One tank contained the epoxy/E-glass coupons and was maintained at 30°C. The other heated tank contained vinyl-ester/E-glass coupons and is maintained at 40°C. A third unheated tank is used to age both the epoxy and vinyl-ester composites at room temperature. The maximum water circulation around the coupons was allowed while they were supported evenly, so that there were no unwanted stresses generated in specimens during the saturation. Each of the coupons was weighed on a mass balance and the weight recorded before it was placed in the tank. The average weight for the Epoxy/E-glass and Vinylester/E-glass coupons were 43.872g (4.1% variation) and 43.596g (1.4% variation), respectively. The coupons were re-weighed before testing (after the immersion ageing period) to establish the amount of water that had been absorbed during ageing.

5.2 Stressed Immersed Testing

Fig. 13a shows a vinyl-ester/E-glass coupon installed in a stressed test configuration. The main component of this rig is a heavy duty die spring (Berger R50-203, Berger Tools Ltd., Kemsing, Kent, UK), with a spring rate of 117 N/mm. The end cap of the stressing mechanism transfers the load from the die spring end into stainless steel pin. The end cap has a slot machined in it to allow a 25mm×4mm coupon to pass through. The coupon was modified slightly to work with the mechanism by having an 8mm hole drilled in each end. During assembly of the mechanism the spring was compressed by 34.2 mm and trapped

between the end caps and pins inserted in the holes in the coupon, thereby applying a 4kN load to the composite coupon. This resulted in a stress of 42.7 MPa and a strain of 0.21 % in the 25×3.75mm QI vinyl-ester/E-glass coupons. Before each of the ten coupons are assembled into the stressing rig, they were fatigued in air for 10,000 cycles between 0.8 kN and 8 kN. This load level was chosen to cause cracking in the 90° plies of the material in order to mimic the damage expected to occur in service. Five of the stressed coupons were immersed in 40°C water for 20 months, while the other five were stored in insulated conditions at the same temperature as the water bath. The fatigue testing setup is shown in Fig. 13b while the testing procedure is described in Section 4.2.

Fig. 13 a) Stressing mechanism for stress ageing of GFRP coupon and b) Immersed fatigue test setup, polyethylene pouch with waterproof tape.

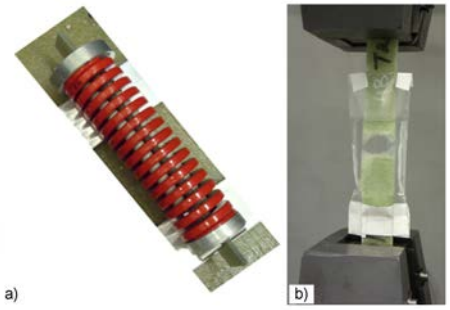

5.3 Water uptake during immersion ageing

The rate of water absorbtion at 30°C and 20°C (room temperature) by the epoxy/E-glass coupons is shown in Figure 14a. The results show that the coupons immersed in the 30°C aging tank absorbed water more quickly than those at room temperature, becoming saturated at 0.6% moisture. This is expected as the higher temperature in the aging tank triggers the higher diffusion of the water molecules. On the contrary, the coupons at room temperature had not become saturated by the end of the immersion period. The results of the vinyl-ester/E-glass coupons immersion show the same trend (Fig. 14b). The vinyl-ester/E-glass coupons immersed in 40°C water for 21 months on average absorbed 0.16% of their weight. As previously observed, the lower immersion temperatures resulted in slower saturation of the specimens.

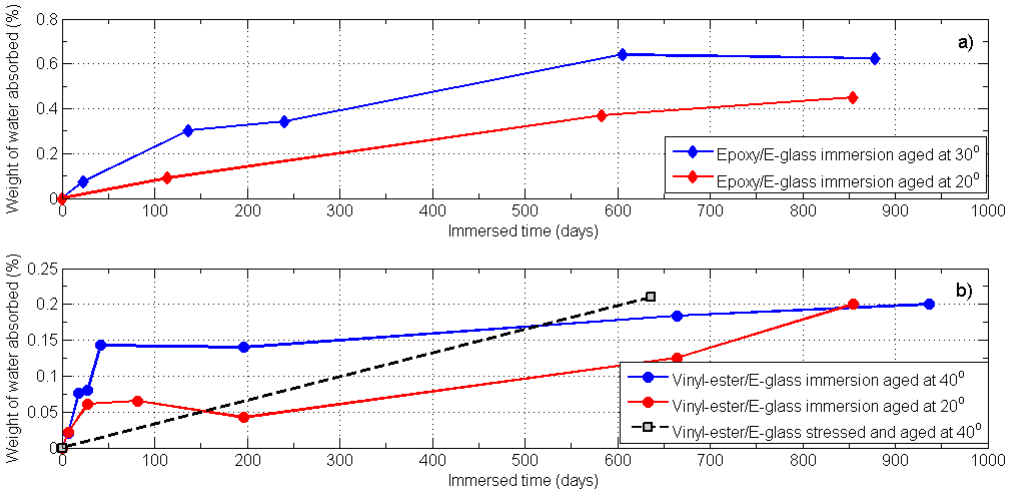

Fig. 14 Weight of water absorbed by: a) Epoxy/E-glass and b) Vinyl-ester/E-glass composite during water immersion ageing.

The amounts of water absorption by the epoxy and vinyl-ester composite coupons are significantly lower than previously reported in the literature [39; 40]. There are two possible reasons why this phenomenon occurred: a) the particular polymers chosen for this work are for use in immersed applications, thus they have been developed to minimise water absorption, and b) the laminates from which the coupons were taken had a low void content.

5.4 Effects of Water Saturation on Fatigue Life of E-glass/Epoxy

Constant amplitude fatigue testing of both dry and wet coupons established the stress-life curves for the materials and thereby quantified the degradation in the fatigue strength due to to water saturation of the materials. The results of fatigue testing epoxy/E-glass QI coupons in tension-tension mode (R=0.1) for the wet and dry coupons is shown in Fig. 15. The dry coupons were stored at room temperature for 20 months and tested in air at room temperature, while the wet coupons were immersed for 20 months in 30° C water and tested while immersed, in the water pouch (Fig. 13b), at room temperature. The results show a drop in fatigue strength for the water aged and immersed coupons compared to the coupons which were aged and tested in normal room temperature air. At high stresses the wet aged fatigue strength decreases by 20 to 25% and at high cycles the wet aged strength is 8% below the fatigue strength of the dry material. The actual change in fatigue life of a structure will depend on the spectrum of fatigue cycles loads it experiences while it is in service. It is observed that during fatigue testing all the immersed coupons broke in the zone that was actually immersed in water within the pouch which indicates that it is important to keep the coupons wet during testing for best representation of the immersed failure condition, as any drying that takes place during the testing tends to be accompanied by a recovery in strength.

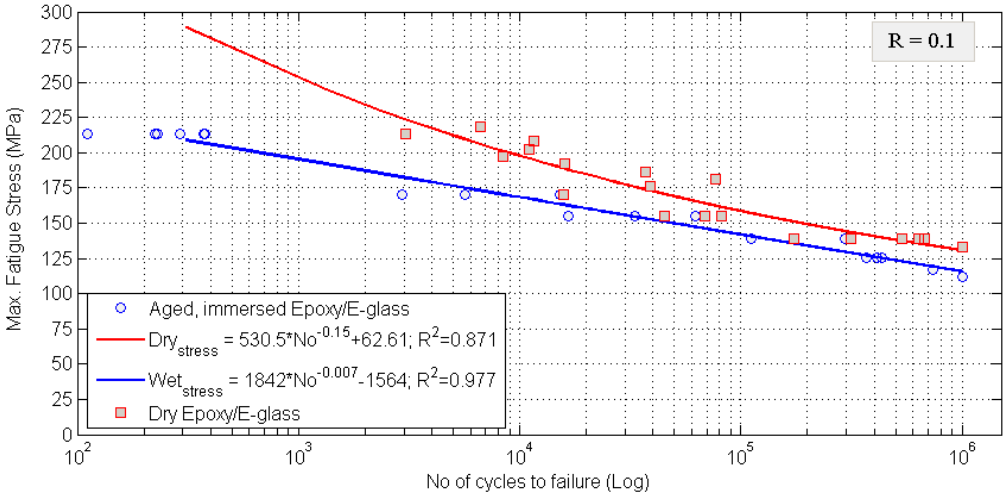

Fig. 15 Stress-life curves for wet and dry epoxy/E-glass in R=0.1 fatigue tests.

5.5 Fatigue Modulus Reduction in Wet and Dry GF/Epoxy

The fatigue modulus is monitored during the fatigue tests on the dry and wet coupons. The evolution in fatigue modulus over the life of wet and dry coupons at three different load levels shows that wet coupon stiffness decays in the same way as the dry coupons during fatigue cycling (Fig. 16). The only significant difference between the behaviour of the wet and dry coupons during fatigue cycling is that the wet coupons consistently fail at a lower number of cycles.

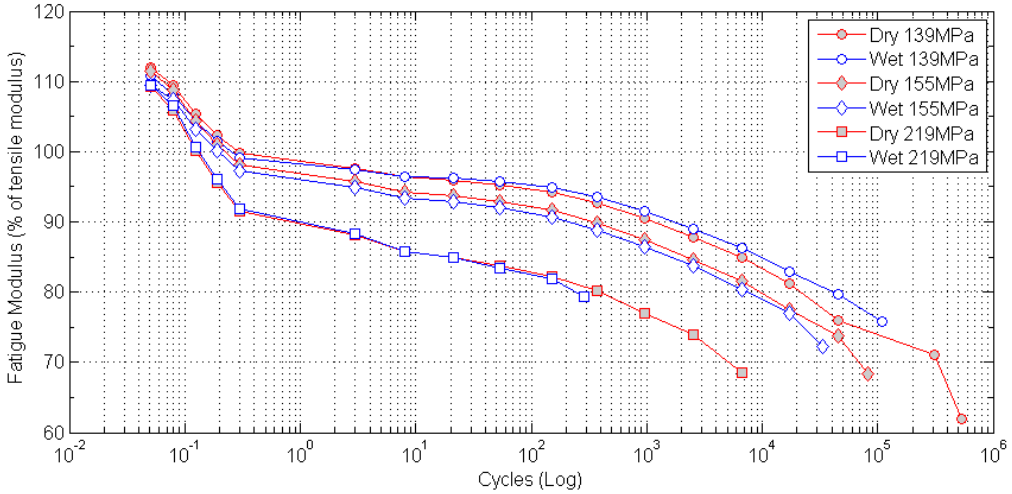

Fig. 16 QI epoxy/E-glass Modulus degradation during fatigue cycling at R=0.1

6 Tidal Turbine Blade Design Example

6.1 Tidal Blade Model

The following design example is based on 3-bladed downstream, free-yaw tidal device with a 5.0 m rotor radius, operating in a 2.6 m/s tidal current velocity, and with approximately 330 kW production capacity. The input parameters for the HDM (generated by tidal model) are shown in Table 2.

Table 2. Parameters for base case hydrodynamic model

Parameter	Value
Water velocity	2.6 m/s
Number of blades	3
R_{outer}	5.0 m
RPM	16
C_L	1.0
L/D	70
Angle of attack	7°
ζ	0.333
Water density	1025 kg/m³
Water viscosity	0.0013155 Pa.s
R_{inner}	1.5 m

6.2 Hydrodynamic model

The algorithm of the HDM, as described in Section 2.4, is shown in Fig. 17. The design of the aerofoil (chord and twist distribution along the blade) is found so that the turbine has the optimum performance over its lifetime. The blade is devided on numer of sections (stream tubes). The HDM performs adjustments of the chord length until the moment balance is achieved, after which the process is repeated for all remaining stream tubes. For the set of input parameters (Table 2) model generates the radial distribution of blade chord length, pitch angle, tangential and axial forces, and power. In this example, the chord length at the blade root is 1.25m with the pitch angle 20°, while the chord length at the tip is 0.75m

with the pitch angle 4°. F_A increases linearly with increasing radius, from 0.7kN to 2.3kN at the extreme blade radius, and is significantly larger than the (power-generating) F_C, which increases with the radius from 320N to 410N at the extreme blade radius (Fig. 6). These forces cause a flapwise bending moment of 150kNm and edgewise bending moment of 35.7kNm, respectively, at a 1.5m radius from the rotor centre.

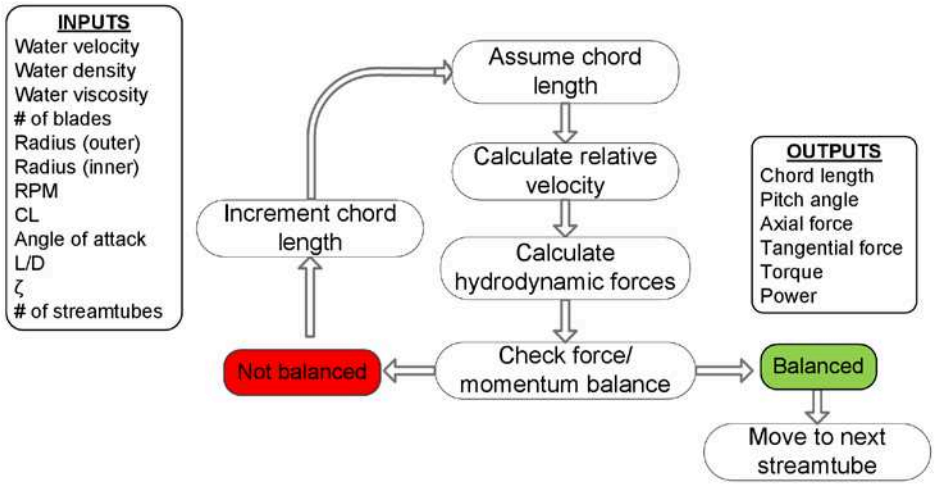

Fig. 17 Summary of hydrodynamic model method.

6.2.1 Pitch Regulated Tidal Turbines

In order to regulate the turbine power during high water velocity, control systems are used to manage forces and moments on the tidal blade. The HDM is used to simulate the two options for controlling power in tidal turbines, pitch-regulation (PR) and stall-regulation (SR). PR is a system which modifies the lift coefficient (C_L), i.e. the forces on the blade, by rotating the entire blade about its axis. SR blades are designed with a radial variation of pitch angle so that the angle of attack over a section of the blade exceeds the stall angle and lift drops off, reducing the forces on the blade, with tidal velocity increase [41]. An operational range of velocity for tidal currents is typically 0.75 to 3 m/s (exceptionally 4 m/s). For this example the operational environment is such that both control systems produce the same flapwise moment [42].

The maximum theoretical power levels for SR and PR turbines and the energy produced by each turbine per year are calculated using the HDM [24]. The energy output of the PR turbine is matched to that of the SR turbine to enable an objective comparison with the respect to damage accumulation. This is achieved by identifying the threshold value of water velocity for pitch control, above which blade pitch is controlled to give constant power. Fig. 18a and 18b shows the power and thrust moment curve for a PR and SR tidal turbine, respectively. These turbines would have similar energy output in a year at 3.05 m/s current speed.

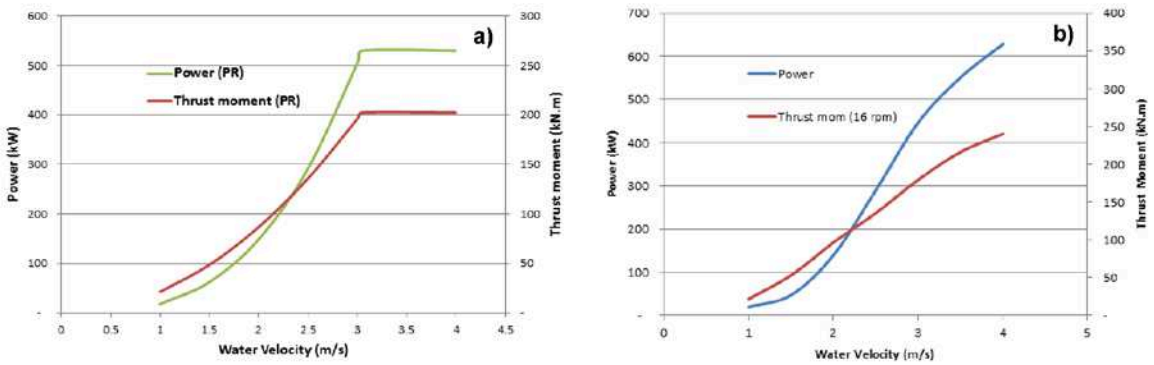

Fig. 18 Power and thrust moment of a) Pitch- and b) Stall-regulated tidal turbine operating in different flow regimes.

6.2.2 Effect of Control Strategy on Bending Moments

The maximum fibre strain at any water velocity, given the flapwise bending moment at that water velocity and the assumption of linear elasticity in the blade, can be computed using equation (5) given in Section 2.7. The predicted dependence of bending moment near the root of the blade on water velocity, due to thrust forces calculated by the HDM, for a PR, an SR and an unregulated tidal turbine is shown in Fig.19. The turbines operate in the water velocity regime where all three control systems produce the same flapwise moment (Section 6.3).

Fig. 19 Predicted effect of water velocity on blade bending moment (at R=1.5m) for various control strategies, as calculated using hydrodynamic model.

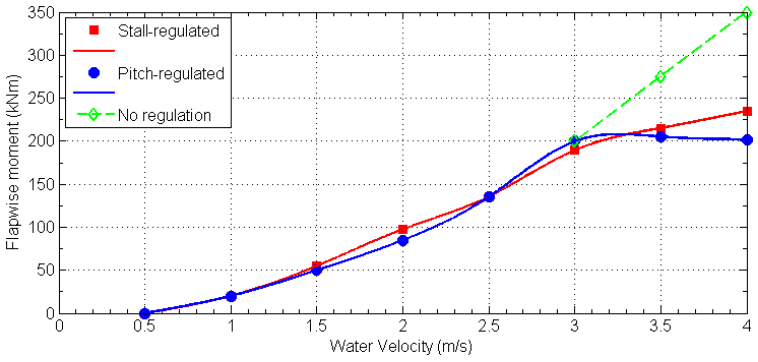

6.3 Structural / Finite Element Model

The aerofoil shape has been simplified (Fig. 20a) for structural modelling, by a piecewise linear equivalent keeping the same section thickness, 24% of chord length (Fig. 20b). The two shear webs have been inserted into the aerofoil shape creating a box section which becomes the structural core of the blade. The top caps and shear webs of the box are 35 and 12 mm thick near the root (at 1.5 m radius) and taper to 6 and 4 mm at the tip, respectively. A finite element (FE) model of a tidal turbine blade has been created using Abaqus FEA software [43] (Fig. 20c) with the panels of the blade modelled as shell elements with QI material properties from standard laminate analysis [44] (Table 3).

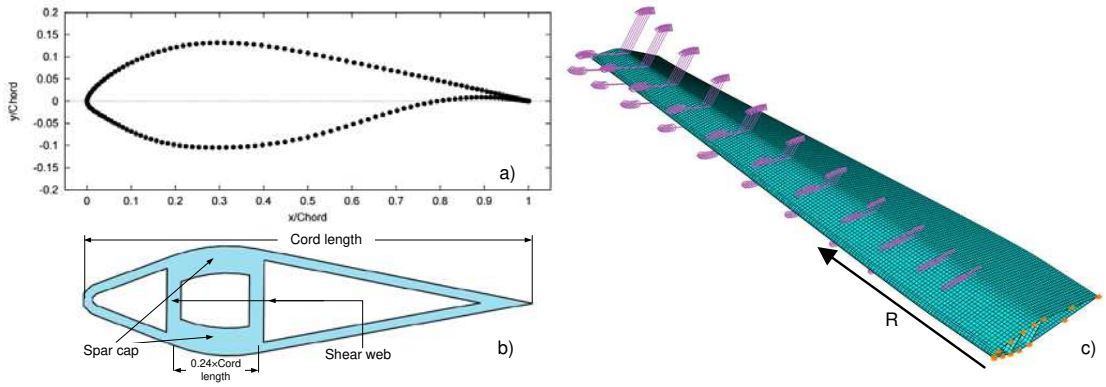

Fig. 20 a) RIS-A1-24 Airfoil [45]; b) Simplified aerofoil shape used for finite element analysis of a tidal turbine blade and c) Final element (FE) model of a 5 m blade for a 3-bladed, 330kW turbine.

Table 3. Epoxy/E-glass material properties.

Inputs		**Single unidirectional ply properties**		**Quasi-isotropic laminate $[(45\backslash 135\backslash 90\backslash 0)_2]_s$**	
V_f	50%	E_1	38 GPa	E_x, E_y	19.3 GPa
E_f	72.4 GPa	E_2	11.6 GPa	G_{xy}	7.2 GPa
ν_f	0.22	G_{12}	3.5 GPa	ν_{xy}	0.330
E_m	3.5 GPa	ν_{12}	0.285		
ν_m	0.35				

The deflected shape of the blade for the extreme loading, taking into account a safety factor of 2, applied to the FE model is shown in Fig. 21. Under the factored load the blade tip deflects 334mm axially, which is approximately twice the blade aerofoil thickness at the tip. This amount of deflection will not introduce any significant error into either the structural or hydrodynamic calculations [24].

Fig. 21 Undeformed and deformed shape of blade at 2.6 m/s water velocity, with a factor of safety of 2.0 applied

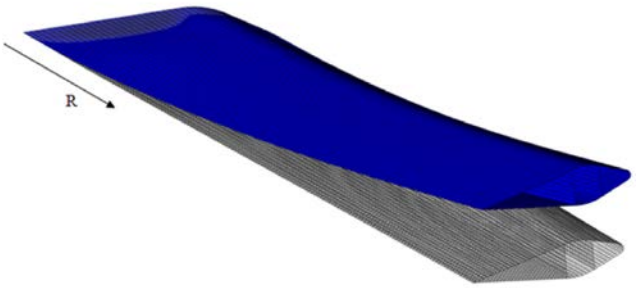

In order to predict fatigue damage accumulation, using equations given in Sections 2-4, the moment-velocity relationships (Fig. 19) are fitted with polynomial expressions, to allow interpolation with respect to water velocity. The fatigue reference case (Table 4) is analysed by the fatigue model which predicted a fatigue life of 11.6 years for the observed case scenario. The fatigue model (Section 2.7) can give insight into the effects of each of the parameters shown in Table 4, on the fatigue life.

Table 4. Parameters for fatigue reference case.

Parameter	Value
Maximum Water Velocity	4.0m/s
Neap max. velocity / Spring max. velocity	60%
Factor of safety applied to loads	2
Tower shadow	50%
Control system	PR
Material	Epoxy/E-glass
Spar top cap thickness range	35mm – 6mm
Shear web and fairings thickness range	12mm – 4mm

The results of the FE analysis show that the highest stresses and strains occur near the blade root, in the spar caps of the structural beam box section (Fig. 22). These are primarily caused by the large (flapwise) bending moments due to the thrust force, F_A (Fig. 6).

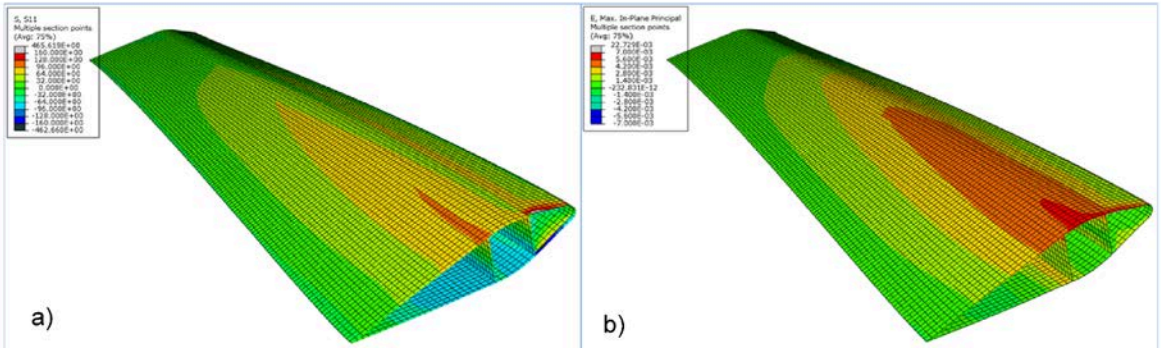

Fig. 22 Final element model results; a) First principal stress distribution in 45° surface ply under design load and b) Maximum principal strains in the outer surface along the blade under design load.

The maximum bending strains occur on the outer surface, while the maximum principal strains are in the middle of the spar cap. In order to make an appropriate comparison to the experimental fatigue life data, it is necessary to find the maximum fibre strain in a ply in which the fibres are closely aligned to the load direction (note that surface ply is 45° to the blade axis). Fibre strains along a section through the midline of the pressure side spar cap extending from near the hub to the tip of the blade are shown in Fig. 23. The fibres in the three outermost plies are at 45°, 135° and 90° to the blade axis (i.e. to the maximum principal strain) which reduces their fibre strains. The 4th ply from the surface has its fibres at 0° to the blade axis which means that is aligned with the direction of the principal bending strains. The maximum fibre strains are predicted in this ply (Fig. 23).

Fig. 23 Fibre strains in the four outermost plies at maximum strain locations along blade operating in 2.6m/s water velocity.

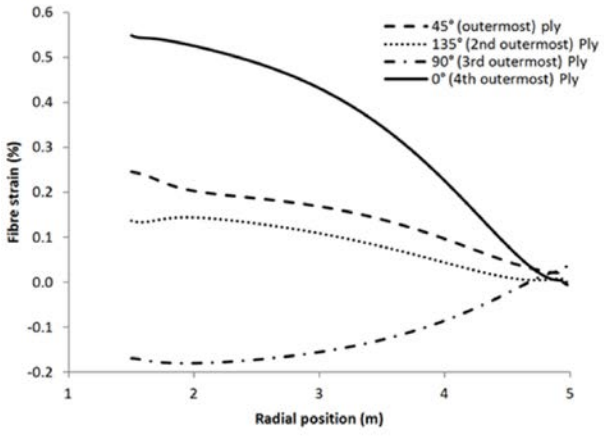

The base case results have given the maximum fibre strain in the turbine blade at 2.6 m/s water velocity. To compute maximum fibre strain at any water velocity, given the flapwise bending moment at that water velocity with the assumption of linear elasticity in the blade, equation (5) can be employed.

6.4 Composite Damage (Pitch vs Stall Regulation)

The blade life of SR and PR devices is determined using the fatigue model. Based on the water velocity increments of 0.1m/s the fatigue damage fraction for each rotation of the turbine is calculated. The results of cumulative damage for the PR and SR blades for different velocities is presented in Fig. 24. The area under each individual curve represents the normalized total accumulated damage over the blade's lifetime.

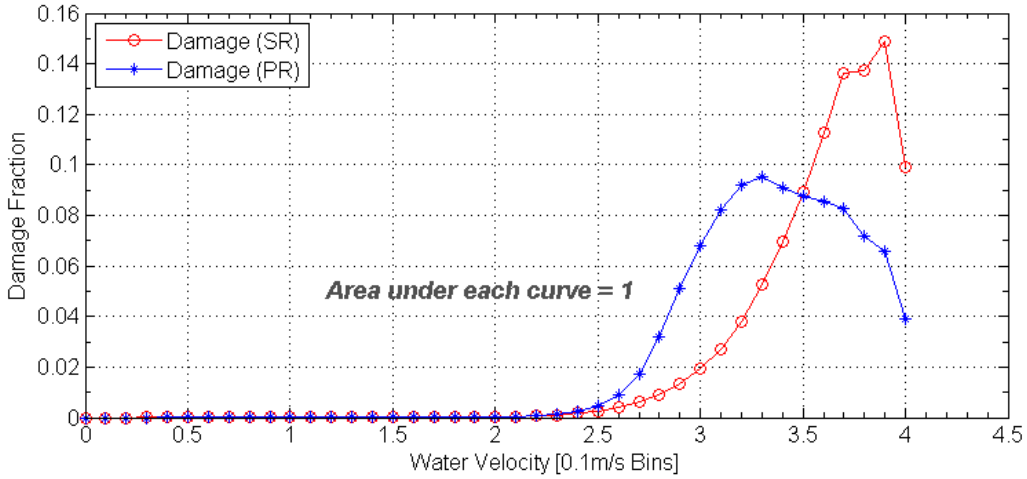

Fig. 24 Damage accumulation per 0.1m/s bin for PR and SR epoxy/E-glass turbine blades operating in a tidal flow with 4.0m/s maximum velocity and 60% neap/spring variation.

The bulk of the damage that occurs in the SR blade is at high water velocities (greater than 3.5m/s). On the contrary, the PR blade experiences more damage at low water velocities. For example, the damage fractions of SR and PR turbine blades at 3.9m/s water velocity are 0.149 and 0.066, respectively. The reason for the SR turbine blade's behaviour at such high velocities is the relatively higher bending strain in comparison with the PR blade. However, the PR blade experiences the most of the damage at medium water valocities (2.5 – 3.5m/s). This is consistant with the fact that PR blades predominately operate in this water regime. Hence, when comparing the blades with the same structural design, employed on two differently controlled tidal turbine devices it was found that the SR blade has a shorter life span (12.8 years) than PR blade (20years).

7 Effect of Water Saturation on Predicted Blade Fatigue Life

The predicted fatigue life for a blade on a SR and PR tidal turbine is plotted against maximum stress experienced by the blade in a 2.5 m/s tidal flow (Fig. 25). The predicted 20 year "dry" fatigue life of a stall-regulated tidal turbine blade is reduced to 17 years if the laminate is water saturated. For a 66 MPa maximum stress in the blade, the predicted "dry" life is 5 years and the predicted "wet" life is 2.9 years. Kennedy et al. have shown that a stall-regulated blade with "dry" laminates need only have 10% thicker laminates in order to

have equal life with a pitch-regulated blade [24]. However, the analysis shows that the laminates would need to be an additional 1 to 4% thicker to counteract the effects of water saturation on the blade. A blade of PR turbine with a maximum stress of 72MPa, which is predicted to have a 5 year "dry" life, will fail, on average, 1.7 years earlier if the blade laminates are water saturated. However, the "dry" life of 20 years and the "wet" life of 19.1 years when water saturated can be achived by increasing the thickness of the laminates, and thus reducing the stress in the blade to 63.5MPa. This convergence of the wet and dry laminate lives occurs because pitch regulation limits the maximum stress in the blades. In achieving the longer blade fatigue life (>15 years), stresses are limited to levels where the difference in life between wet and dry laminates is very small. According to the results shown in Fig. 25, the life of water saturated blades is reduced by about 3 years for SR and about 1-2 years for PR turbines.

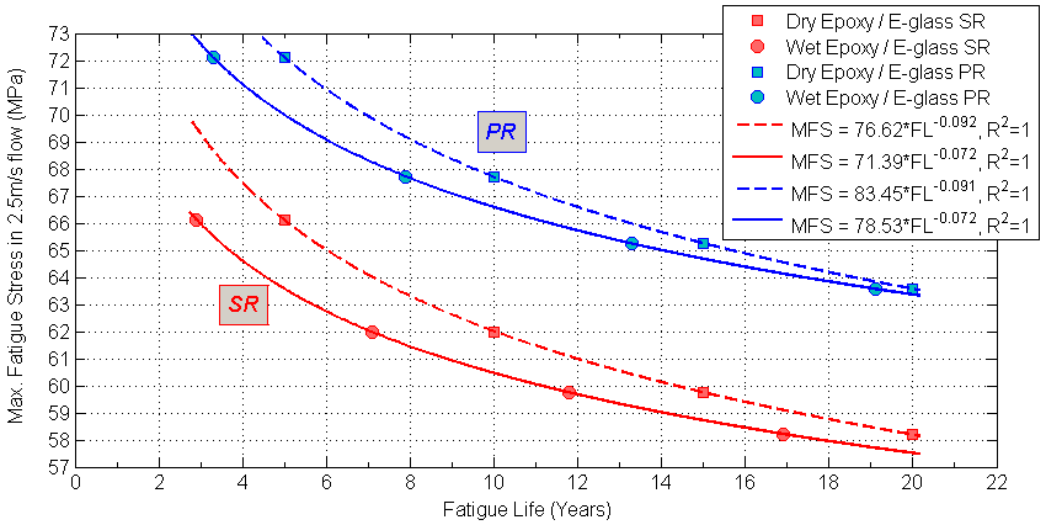

Fig. 25 Effect of seawater saturation on predicted fatigue life of pitch-regulated (PR) and stall-regulated (SR) tidal turbine blades.

8 Conclusions

An approach for the fundamental fatigue design of Glass Fibre Reinforced Polymer (GFRP) tidal turbine blades is described in this study. The model is implemented with the aim to estimate and compare the immersed life of Stall-Regulated (SR) and Pitch-Regulated (PR) tidal turbine blades. In that regard, the uniaxial fatigue testing results of water-immersed Quasi-Isotropic (QI) GFRP, i.e epoxy/E-glass and vinyl-ester/E-glass materials, are incorporated in the three-bladed tidal turbine model for a range of tidal velocities.

The mechanical properties of the material used in the blades is evaluated. There was only 1% drop in QI epoxy/E-glass coupons modulus when immersed in 30°C for 20 months. However, there was no difference between the fatigue modulus for the wet and dry specimens. For the increased water temperature the water absorption was relatively low, i.e. for epoxy/E-glass (0.6% for 20 months at 30°C) and vinyl-ester/E-glass (0.2% for 22 months at 40°C). Regardless of the low level of water absorption, the fatigue strength of the material was significantly degraded by water immersion-ageing. It was found that the wet fatigue strength is 20% and 8% lower than the dry fatigue strength at 1,000 cycles and at 1 million cycles, respectively. Hence, the effect of water saturation is also stress level dependent. The stressing of the coupons during immersion did not result in additional water absorption. However, these specimens experienced 10% loss in fatigue strength. Overall, it is found that

the epoxy/E-glass material is significantly more fatigue resistant than the vinyl-ester/E-glass material and thus more desirable in tidal blade design.

Nonetheless, the experiments showed that the fatigue life of tidalblades is extensively dependant on strain-stress level experienced by the blade, regardless of the material. For instance, an increase in a material stress of only 15% could decrease blade life by up to 75%. Likewise, the tower-shadow effect influences the fatigue life of blades, so that increasing the shadow effect from 50% to 90% will lead to 15% reduction in the blade fatigue strength or maximum allowable strain. Regarding tidal turbine blade life span, the study found that an SR blade will have a shorter life than an equivalent PR turbine blade. In order to increase the fatigue blade life of the SR blade to that of PR turbine blade, the thickness of the laminates in the spar cap need to be increased by aproximately 10%, i.e. decresing the maximum strain by about 5%. However, in the case of both devices, the laminates in the spar need to be between 1% and 4% thicker inorder to prevent the negative effect of water saturation on the blade.

Acknowledgements

The authors would like to acknowledge funding from Science Foundation Ireland (SFI) through the Advance Award (14/ADV/RC3022) and the Marine and Renewable Energy Ireland (MaREI) Centre, Grant No. 12/RC/2305; and from the European Union under Framework 7, through the MARINCOMP Project, Grant agreement no.: FP7-612531.

References

1. NASA. (2016). TOPEX/Poseidon: Revealing Hidden Tidal Energy. Retrieved 14.10.2016, 2016, from http://svs.gsfc.nasa.gov/stories/topex/tides.html
2. UKCE. (2012). *UK Wave and Tidal Key Resource Areas Project Summary Report* The Crown Estate Retrieved from https://www.thecrownestate.co.uk/media/5476/uk-wave-and-tidal-key-resource-areas-project.pdf.
3. SEI. (2006). Tidal and Current Energy Resources in Ireland Report. Dublin, Ireland.
4. Magagna, D., & Uihlein, A. (2015). Ocean energy development in Europe: Current status and future perspectives. *International Journal of Marine Energy, 11*, 84-104. doi: http://dx.doi.org/10.1016/j.ijome.2015.05.001
5. O'Rourke, F., Boyle, F., & Reynolds, A. (2010). Tidal current energy resource assessment in Ireland: Current status and future update. *Renewable and Sustainable Energy Reviews, 14*(9), 3206-3212.
6. Little, C., Grimwade, J., & Court, R. S. (2012). *Recommendations on the Structural Testing Requirements for Tidal Stream Blades* Paper presented at the ICOE2012, Dublin, Ireland. https://www.icoe-conference.com/publication/recommendations_on_the_structural_testing_requirements_for_tidal_stream_blades/
7. Jaksic, V., Kennedy, C. R., Leen, S. B., & Brádaigh, C. M. Ó. (2016, 21-22 March). *Tidal Turbine Blade Design from a Fatigue Point of View*. Paper presented at the Oxford Tidal Energy Workshop, OTE2016, Department of Engineering Science, Oxford, UK.
8. Davies, P., & Rajapakse, Y. D. S. (2014). *Durability of composite in marine environment* (Vol. 208): Springer.
9. Grogan, D., Leen, S., Kennedy, C., & Brádaigh, C. O. (2013). Design of composite tidal turbine blades. *Renewable Energy, 57*, 151-162.
10. Fagan, E. M., Kennedy, C. R., Leen, S. B., & Goggins, J. (2016). Damage mechanics based design methodology for tidal current turbine composite blades. *Renewable Energy, 97*, 358-372. doi: http://dx.doi.org/10.1016/j.renene.2016.05.093
11. *MARINCOMP: EU FP 7 Marie Curie IAPP Project MARINCOMP – "Novel Composite Materials and Processes for Marine Renewable Energy", Grant agreement number: FP7-*

612531, Funded under: FP7-People. www.marincomp.eu.
12. Baba, N. B., Suhaimi, A. S., Mohd Amin, M. A., & Mohd, A. (2015). Study on Mechanical and Physical Behaviour of Hybrid GFRP. *Advances in Materials Science and Engineering, 2015*, 7. doi: 10.1155/2015/138965
13. Kennedy, C. R., Leen, S. B., & Ó Brádaigh, C. M. (2016). Immersed Fatigue Performance of Glass Fibre-Reinforced Composites for Tidal Turbine Blade Applications. *Journal of Bio- and Tribo-Corrosion, 2*(2), 1-10. doi: 10.1007/s40735-016-0038-z
14. Degrieck, J., & Van Paepegem, W. (2001). Fatigue damage modeling of fibre-reinforced composite materials: Review. *Applied Mechanics Reviews, 54*(4), 279-300.
15. DNV GL – Energy. (2014). Horizontal axis tidal turbines *Renewables Certification – Wave and Tidal* (pp. 284).
16. DNVGL. (2015). Tidal turbines - Rules and standards.
17. Vassilopoulos, A. P., Manshadi, B. D., & Keller, T. (2010). Influence of the constant life diagram formulation on the fatigue life prediction of composite materials. *International Journal of Fatigue, 32*(4), 659-669. doi: http://dx.doi.org/10.1016/j.ijfatigue.2009.09.008
18. Duan, X., & Yao, W. X. (2002). Multi-directional stiffness degradation induced by matrix cracking in composite laminates. *International Journal of Fatigue, 24*(2–4), 119-125. doi: http://dx.doi.org/10.1016/S0142-1123(01)00066-4
19. Talreja, R. (2013). *Continuum modeling of the development of intralaminar cracking in composite laminates.* Paper presented at the ICF7, Houston (USA) 1989.
20. McCann, G. N., Rawlinson-Smith, R. I., & Argyriadis, K. (2006). *Load Simulation for Tidal Turbines using Wind Turbine Experience.* Paper presented at the ICOE'06, Bremerhaven, Germany.
21. Bahaj, A. S., Batten, W. M. J., & McCann, G. (2007). Experimental verifications of numerical predictions for the hydrodynamic performance of horizontal axis marine current turbines. *Renewable Energy, 32*(15), 2479-2490. doi: http://dx.doi.org/10.1016/j.renene.2007.10.001
22. Batten, W., Bahaj, A., Molland, A., Chaplin, J., & Group, S. E. R. (2007). Experimentally validated numerical method for the hydrodynamic design of horizontal axis tidal turbines. *Ocean Engineering, 34*(7), 1013-1020.
23. Bahaj, A., Molland, A., Chaplin, J., & Batten, W. (2007). Power and thrust measurements of marine current turbines under various hydrodynamic flow conditions in a cavitation tunnel and a towing tank. *Renewable Energy, 32*(3), 407-426.
24. Kennedy, C. R., Leen, S. B., & Brádaigh, C. M. Ó. (2012). A preliminary design methodology for fatigue life prediction of polymer composites for tidal turbine blades. *Proceedings of the Institution of Mechanical Engineers, Part L: Journal of Materials Design and Applications*, 1464420712443330.
25. Jaksic, V., Kennedy, C. R., Leen, S. B., & Brádaigh, C. M. Ó. (2016, 21-22 March). *Tidal Turbine Blade Design from a Composite Fatigue Point of View.* Paper presented at the 5th Oxford Tidal Energy Workshop, Oxford, UK.
26. Bryans, A. G., Fox, B., Crossley, P. A., & O'Malley, M. (2005). Impact of tidal generation on power system operation in Ireland. *IEEE Transactions on Power Systems, 20*(4), 2034-2040.
27. Pugh, D. T. (1988). *Tides, Surges, and Mean Sea-Level/a Handbook for Engineers and Scientists*: John Wiley & Sons Inc.
28. Tidal Observations - Irish National Tide Gauge Network. (2016). from Marine Institute http://www.marine.ie/Home/site-area/data-services/real-time-observations/tidal-observations
29. Batten, W. M. J., Bahaj, A. S., Molland, A. F., & Chaplin, J. R. (2008). The prediction of the hydrodynamic performance of marine current turbines. *Renewable Energy, 33*(5), 1085-1096. doi: http://dx.doi.org/10.1016/j.renene.2007.05.043
30. Batten, W. M. J., Bahaj, A. S., Molland, A. F., & Chaplin, J. R. (2006). Hydrodynamics of marine current turbines. *Renewable Energy, 31*(2), 249-256. doi: http://dx.doi.org/10.1016/j.renene.2005.08.020
31. UIUC. (2016). Airfoil Data Set. Illinois, USA: University of Illinois at Urbana–Champaign (UIUC), Applied Aerodynamics Group
32. NREL. (2012). PreComp: National laboratory of the U.S. Department of Energy, Office of

Energy Efficiency and Renewable Energy. Retrieved from https://nwtc.nrel.gov/PreComp
33. Segovia, F., Salvador, M. D., Sahuquillo, O., & Vicente, A. (2007). Effects of Long-term Exposure on E-glass Composite Material Subjected to Stress Corrosion in a Saline Medium. *Journal of Composite Materials, 41*(17), 2119-2128. doi: 10.1177/0021998307074134
34. Bir, G. S. (2006). User's Guide to PreComp (Pre-Processor for Computing Composite Blade Properties). Colorado, USA: National Renewable Energy Laboratory (NREL).
35. Barltrop, N., Varyani, K., Grant, A., Clelland, D., & Pham, X. (2006). Wave-current interactions in marine current turbines. *Proceedings of the Institution of Mechanical Engineers, Part M: Journal of Engineering for the Maritime Environment, 220*(4), 195-203.
36. Gamstedt, E. K., & Sjögren, B. A. (2002). An experimental investigation of the sequence effect in block amplitude loading of cross-ply composite laminates. *International Journal of Fatigue, 24*(2–4), 437-446. doi: http://dx.doi.org/10.1016/S0142-1123(01)00099-8
37. Kennedy, C. R., Brádaigh, C. M. Ó., & Leen, S. B. (2013). A multiaxial fatigue damage model for fibre reinforced polymer composites. *Composite Structures, 106*, 201-210.
38. Purnell, P., Cain, J., Van Itterbeeck, P., & Lesko, J. (2008). Service life modelling of fibre composites: A unified approach. *Composites Science and Technology, 68*(15), 3330-3336.
39. Davies, P., Mazeas, F., & Casari, P. (2001). Sea water aging of glass reinforced composites: shear behaviour and damage modelling. *Journal of Composite Materials, 35*(15), 1343-1372.
40. Narasimha Murthy, H. N., Sreejith, M., Krishna, M., Sharma, S. C., & Sheshadri, T. S. (2010). Seawater Durability of Epoxy/Vinyl Ester Reinforced with Glass/Carbon Composites. *Journal of Reinforced Plastics and Composites, 29*(10), 1491-1499. doi: 10.1177/0731684409335451
41. Whitby, B., & Ugalde-Loo, C. E. (2014). Performance of Pitch and Stall Regulated Tidal Stream Turbines. *Sustainable Energy, IEEE Transactions on, 5*(1), 64-72. doi: 10.1109/TSTE.2013.2272653
42. Carr, R. (July, 2010). [Tide height data. (personal communication)].
43. SIMULIA. (2010). "Abaqus FEA". Dassault Systèmes. from http://www.3ds.com/products-services/simulia/products/
44. Crawford, R. J. (1998). *Plastics engineering*: Butterworth-Heinemann.
45. Bertagnolio, F., Sørensen, N. N., Johansen, J., & Fuglsang, P. (2001). Wind turbine airfoil catalogue. Roskilde, Denmark: Riso National Laboratory.